Measurement of resonant bend loss in anti-resonant hollow core optical fiber

Research Article | Vol. 25, No. 17 | 21 Aug 2017 | OPTICS EXPRESS 20612
Optics EXPRESS

Measurement of resonant bend loss in anti-resonant hollow core optical fiber

RICHARD M. CARTER,[1,*] FEI YU,[2] WILLIAM J. WADSWORTH,[2] JONATHAN D. SHEPHARD,[1] TIM BIRKS,[2] JONATHAN C. KNIGHT,[2] AND DUNCAN P. HAND[1]

[1]*Institute of Photonics and Quantum Sciences, Heriot-Watt University, Edinburgh EH14 4AS, UK*
[2]*Centre for Photonics and Photonic Materials, Department of Physics, University of Bath, BA2 7AY, UK*
[*]*R.M.Carter@hw.ac.uk*

Abstract: We present the results of measurements of resonant spectral bend loss using a novel apparatus in a series of hollow core anti-resonant optical fibers, important for their applications in the delivery of industrial power ultra-short laser pulses. The measured bend losses exhibit clear wavelength-bend diameter resonances. We demonstrate, in good agreement with theoretical analysis, that the sensitivity to bend diameter (in terms of minimum bend radii) is dependent on the ratio between cladding and core structure size. By decreasing the cladding capillary diameter: core diameter ratio from 0.70 to 0.43 the minimum bend diameter is decreased from >160 mm to ~15 mm at a wavelength of 800 nm. Furthermore it is demonstrated that the exact position of the loss bands is highly dependent on the orientation of the fiber structure with the bend plane.

OCIS codes: (060.2270) Fiber characterization; (060.2310) Fiber optics; (060.2400) Fiber properties; (060.4005) Microstructured fibers; (060.2280) Fiber design and fabrication.

References and links

1. A. D. Pryamikov, A. S. Biriukov, A. F. Kosolapov, V. G. Plotnichenko, S. L. Semjonov, and E. M. Dianov, "Demonstration of a waveguide regime for a silica hollow-core microstructured optical fiber with a negative curvature of the core boundary in the spectral region > 3.5 μm," Opt. Express **19**(2), 1441–1448 (2011).
2. F. Yu and J. C. Knight, "Negative curvature hollow core optical fiber," IEEE J. Sel. Top. Quantum Electron. **22**(2), 4400610 (2015).
3. Y. Y. Wang, N. V. Wheeler, F. Couny, P. J. Roberts, and F. Benabid, "Low loss broadband transmission in hypocycloid-core Kagome hollow-core photonic crystal fiber," Opt. Lett. **36**(5), 669–671 (2011).
4. J. D. Shephard, A. Urich, R. M. Carter, P. Jaworski, R. R. J. Maier, W. Belardi, F. Yu, W. J. Wadsworth, J. C. Knight, and D. P. Hand, "Silica hollow core microstructured fibers for beam delivery in industrial and medical applications," Front. Phys., 3 (2015).
5. B. Beaudou, F. Gerôme, Y. Y. Wang, M. Alharbi, T. D. Bradley, G. Humbert, J.-L. Auguste, J.-M. Blondy, and F. Benabid, "Millijoule laser pulse delivery for spark ignition through kagome hollow-core fiber," Opt. Lett. **37**(9), 1430–1432 (2012).
6. P. Jaworski, F. Yu, R. R. J. Maier, W. J. Wadsworth, J. C. Knight, J. D. Shephard, and D. P. Hand, "Picosecond and nanosecond pulse delivery through a hollow-core negative curvature fiber for micro-machining applications," Opt. Express **21**(19), 22742–22753 (2013).
7. F. Emaury, C. F. Dutin, C. J. Saraceno, M. Trant, O. H. Heckl, Y. Y. Wang, C. Schriber, F. Gerome, T. Südmeyer, F. Benabid, and U. Keller, "Beam delivery and pulse compression to sub-50 fs of a modelocked thin-disk laser in a gas-filled Kagome-type HC-PCF fiber," Opt. Express **21**(4), 4986–4994 (2013).
8. E. A. J. Marcatili and R. A. Schmeltzer, "Hollow metallic and dielectric waveguides for long distance optical transmission and lasers," Bell Syst. Tech. J. **43**(4), 1783–1809 (1964).
9. A. F. Kosolapov, A. D. Pryamikov, A. S. Biriukov, V. S. Shiryaev, M. S. Astapovich, G. E. Snopatin, V. G. Plotnichenko, M. F. Churbanov, and E. M. Dianov, "Demonstration of CO_2-laser power delivery through chalcogenide-glass fiber with negative-curvature hollow core," Opt. Express **19**(25), 25723–25728 (2011).
10. M. Alharbi, T. Bradley, B. Debord, C. Fourcade-Dutin, D. Ghosh, L. Vincetti, F. Gérôme, and F. Benabid, "Hypocycloid-shaped hollow-core photonic crystal fiber Part II: Cladding effect on confinement and bend loss," Opt. Express **21**(23), 28609–28616 (2013).
11. V. Setti, L. Vincetti, and A. Argyros, "Flexible tube lattice fibers for terahertz applications," Opt. Express **21**(3), 3388–3399 (2013).

#301064 https://doi.org/10.1364/OE.25.020612
Journal © 2017 Received 28 Jun 2017; revised 31 Jul 2017; accepted 5 Aug 2017; published 15 Aug 2017

Optics EXPRESS

12. M. H. Frosz, P. Roth, M. C. Günendi, and P. S. J. Russell, "Analytical formulation for the bend loss in single-ring hollow-core photonic crystal fibers," Photonics Res. **5**(2), 88–91 (2017).
13. W. Belardi and J. C. Knight, "Effect of core boundary curvature on the confinement losses of hollow antiresonant fibers," Opt. Express **21**(19), 21912–21917 (2013).
14. W. Belardi and J. C. Knight, "Hollow antiresonant fibers with reduced attenuation," Opt. Lett. **39**(7), 1853–1856 (2014).
15. F. Poletti, "Nested antiresonant nodeless hollow core fiber," Opt. Express **22**(20), 23807–23828 (2014).
16. G. K. Alagashev, A. D. Pryamikov, A. F. Kosolapov, A. N. Kolyadin, A. Y. Lukovkin, and A. S. Biriukov, "Impact of geometrical parameters on the optical properties of negative curvature hollow-core fibers," Laser Phys. **25**(5), 055101 (2015).
17. S.-F. Gao, Y.-Y. Wang, X.-L. Liu, W. Ding, and P. Wang, "Bending loss characterization in nodeless hollow-core anti-resonant fiber," Opt. Express **24**(13), 14801–14811 (2016).
18. C. Wei, C. R. Menyuk, and J. Hu, "Bending-induced mode non-degeneracy and coupling in chalcogenide negative curvature fibers," Opt. Express **24**(11), 12228–12239 (2016).
19. C. Wei, C. R. Menyuk, and J. Hu, "Impact of Cladding Tubes in Chalcogenide Negative Curvature Fibers," IEEE Photonics J. **8**(3), 2200509 (2016).
20. M. Michieletto, J. K. Lyngsø, C. Jakobsen, J. Lægsgaard, O. Bang, and T. T. Alkeskjold, "Hollow-core fibers for high power pulse delivery," Opt. Express **24**(7), 7103–7119 (2016).
21. X. Huang, S. Yoo, and K. Yong, "Function of second cladding layer in hollow core tube lattice fibers," Sci. Rep. **7**(1), 1618 (2017).
22. M. Heiblum and J. H. Harris, "Analysis of curved optical waveguides by conformal transformation," IEEE J. Quantum Electron. **11**(2), 75–83 (1975).

1. Introduction

Since 2011 a variety of anti-resonant hollow core fibers (AR-HCFs) have been reported with leakage losses reduced from several dB/m to tens of dB/km or less [1–3]. Low loss combined with low waveguide dispersion, low optical non-linearity and high damage thresholds means that these fibers hold great promise for applications where delivery of high power, and particularly high peak power, laser radiation is required over distances of tens of meters [4].

The relatively simple AR-HCF designs have been the subject of several recent studies into pulsed delivery [4–7] including investigation of the delivered polarization and modal structure.

For most practical applications it is the mechanical flexibility of these fibers that provides a key benefit, thus bend dependent attenuation is a key limiting factor for practical implementation. Due to the leaky nature of the guidance mechanism in AR-HCFs, bend losses increase as bend diameters are decreased due to the reduced reflectivity from the cladding [8]. This form of leakage is inevitable and will occur anywhere the fiber is bent. However the magnitude of these losses can be insignificant in comparison to resonant bend loss occurring at specific, critical, bend diameters.

This resonant bend loss was first predicted in 2011 with a chalcogenide glass AR-HCF [9]. This high loss occurs when phase matching conditions between the core mode and cladding modes are satisfied [9]. For traditional photonic bandgap fibers and 'Kagome' type fiber the large ratio between core and cladding diameters ensures that the core and cladding modes are sufficiently well separated that resonant bend loss only occurs at extremely small bend radii [10]. Setti et al. confirmed the presence of resonant bend losses in AR-HCF made of polymers for THz radiation in 2013 [11]. Since then there have been a number of studies on the phenomenon [11–21]. In 2013 Setti et al. [11] derived the critical radius for bend loss, which was later confirmed by Frosz et al. in 2017 [12]. As a result of these studies a number of fiber designs have been proposed to reduce the critical bend radius by altering the resonance conditions within the fiber [14, 15, 19, 21].

Nevertheless resonant bend loss has only been carefully characterized in an AR-HCF with a six or eight cell design relatively recently, though the bend loss characterization methodology is not thoroughly discussed [16, 17]. In addition, in comparison to the six-cell design, seven-cell AR-HCF has been numerically verified as providing the optimum combination of leakage loss, bend loss and single mode performance required for high power laser delivery applications [20].

Optics EXPRESS

In this paper we describe a new design of bend loss measurement scheme which minimizes the uncertainty of measurement. The resonant bend loss of seven cell AR-HCF is systematically measured and compared with the predictions of the analytical model.

2. Fiber used in this paper

The anti-resonant fiber used in this paper was fabricated by the commonly used stack and draw technique. Seven identical circular capillaries were used to form the cladding of fiber in a preform, which was then drawn down to the final fiber. To control the size and wall thickness of the bounding capillaries and the size of the hollow core, different pressures were applied to the core and the cladding respectively during the fiber drawing process. Four separate fibers were drawn from the same canes with varying ratios between core and cladding ring sizes (Fig. 1 and Table 1). Here the core size is defined as the largest diameter circle fitting into the core region without touching the cladding. Note that as the draw-down ratio changes, the cladding capillary thickness will also change. Since the wall thickness determines the edges of the low-loss window this is different for each of the drawn fibers.

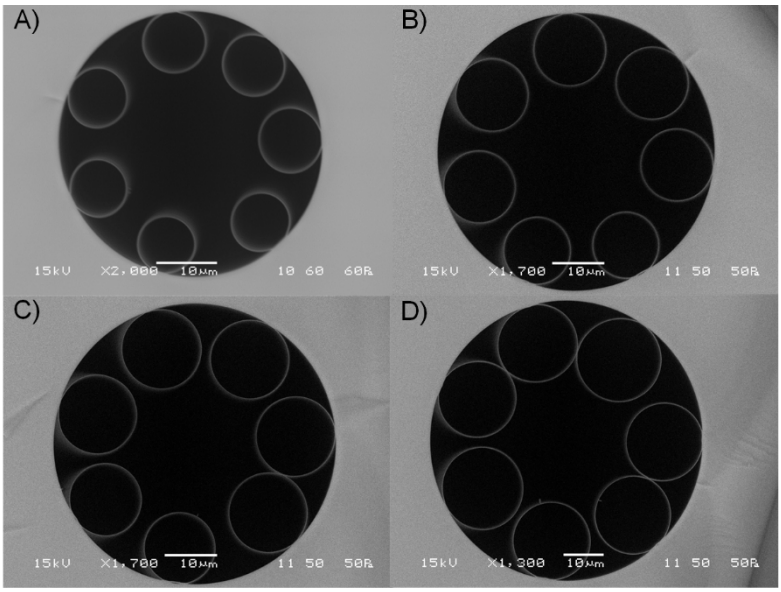

Fig. 1. Scanning Electron Microscope images of the four fibers used in this paper (A, B, C, D), the scale bar in each case is 10 µm.

Table 1. Comparative Core and Cladding Sizes for the Anti-Resonant Fibers Used in this Paper.

Fiber	Core Diameter (µm)	Cladding Diameter (µm)	Cladding capillary: Core Ratio	Outer Diameter (µm)
A	23.2	9.9 ± 0.6	0.43	110
B	25.3	13.6 ± 0.6	0.54	140
C	23.8	14.8 ± 0.8	0.62	140
D	28.4	19.9 ± 0.7	0.70	141

3. Experimental apparatus

A white light tungsten halogen lamp and Ocean Optics spectrometer (S2000 USB, 304 - 1023.5 ~0.3 nm resolution) were used to capture spectra transmitted through each optical fiber as a function of the diameter of an induced single 180° bend. Accurate measurement of the bend dependence of the transmitted spectra requires that two significant conditions must be satisfied:

Optics EXPRESS

(i) That the white light is 100% coupled into the core region and does not propagate in the cladding structure or surrounding glass as these also guide visible light well.

(ii) That a variable bend can be applied to the fiber without introducing additional bends elsewhere in the system which will distort the measurement

The first condition can be satisfied by using a suitable coupling condition for the light into the fiber. In this case light from the lamp was coupled into the core of an SMF-28 fiber using a simple singlet lens. The SMF-28 was then butt-coupled to the test fiber using a three axis microblock (Fig. 2). Although the SMF-28 is not single mode over the wavelength range of interest, its small core size (8 μm) compared to that of the anti-resonant fiber ensures that, when directly coupled, light is selectively launched into the core region. Due to a significant NA mismatch between the two fiber types there is considerable loss when butt-coupling, and a suitable length (> 1m) of fiber is required to strip off residual capillary and surrounding-glass guided light and will act as a filter on higher order core modes (which exhibit higher losses) before the bend region (Fig. 2).

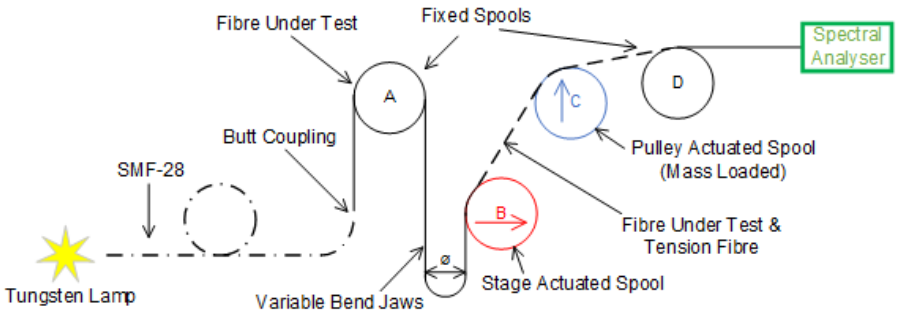

Fig. 2. Schematic of the fiber variable bend diameter apparatus. Light from a tungsten lamp is first coupled into an SMF-28 fiber which is then butt-coupled to the test fiber. The test fiber is looped around spool A, into the test jaws (Fig. 3), then over spools B, C, round spool D and finally into the spectral analyzer. Spool B is attached to the stages controlling the bend diameter in the jaws while spool C is attached to a mass loaded pulley. Thus as the bend diameter increases, and spool B moves to the right, spool C will move upward taking up the increasing fiber slack. An additional length of SMF-28 is wound round spools B, C and D to take the tension from the mass loading of spool C. The purpose of this fiber is purely mechanical, and it plays no optical role.

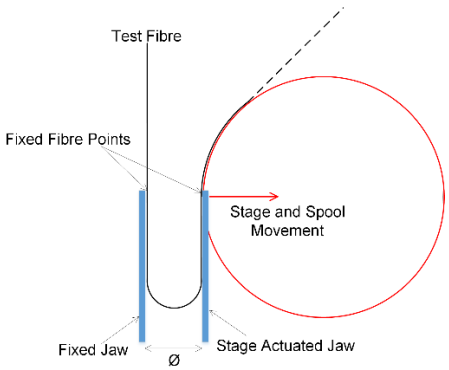

Fig. 3. Schematic of the variable bend jaws from Fig. 2. The fiber is fixed into two jaws with V grooves with tape at the two fixed fiber points.

The second condition is satisfied with careful design of a bending apparatus such that the minimum bend diameter present in the fiber outside of the test bend is sufficiently large to not interfere with the measurement or else is held constant. In our arrangement a series of spools

Optics EXPRESS

with diameter 280 mm are used to limit these additional bends (Fig. 2). This diameter is expected to be sufficiently large to have a negligible effect on the measurement.

The variable bend jaws consist of two metal strips with a 0.1 mm V-groove. One is mounted directly to the optical table while the other is mounted to a Thor Labs LTS – long travel stage. With the fiber held in place within the V-groove by taping to one end (Fig. 3) the separation of the metal strips, and hence the diameter of the half bend, may be varied by moving the stages. In order to prevent the fiber sagging under its own weight as the separation of the jaws increases, the bend plane (and the entire apparatus from butt-coupling to spectral analyzer) is arranged vertically, in line with gravitational forces.

As the distance between the output of the jaws and the spectral analyzer will also change it is necessary to take up the fiber slack. A second spool (Fig. 2 Spool B and Fig. 3) is thus mounted directly onto the variable bend jaws such that the fiber is fed smoothly from the jaws onto the spool. The fiber is then fed round a third spool (Fig. 2 Spool C) which is attached to a mass loaded pulley system which applied force upward. The fiber is then wound once round a fixed spool (Fig. 2 Spool D) where a short straight length of the test fiber is used to connect directly to the spectral analyzer using a temporary fiber terminator (Thor Labs BFT1 & B30250C).

The net effect is that as the jaws increase separation spool B will move to the right while spool C moves upward taking up the slack. As movement in this direction is smoother than the reverse all data was taken with increasing bend diameter.

As we wished to avoid straining the test fiber a second tension fiber (a length of SMF-28) was wound round spool B, over spool C and round spool D to take the strain of the mass loaded spool C (Fig. 2). The test fiber could then be loaded into the apparatus without introducing strain.

Note that the design of the apparatus allows for accurate measurement of the comparatively strong resonant loss bands. The leaky waveguide losses (i.e. 'standard' non-resonant bend losses) are insignificant for a single 180° bend; to measure these losses a large number of turns would be required to generate sufficient loss for accurate measurement. This is not practical with this apparatus without significant re-design.

4. Experimental procedure and data processing

The experimental procedure in all cases was to first mount the fiber into the test rig with the variable test jaws at maximum separation (159.25 mm). This was achieved by first cleaving the fiber at one end and, using the temporary fiber termination, coupling the fiber to the spectral analyzer. The fiber was passed round spool D once and over spools C & B taking care not to strain the fiber in the process (Fig. 2). The fiber was attached with tape to the top of both sides of the variable jaws with sufficient length between to allow the full range of diameters to be tested (Fig. 3).

The remaining fiber was coiled around spool A (Fig. 2) and finally cleaved and butt-coupled to the SMF-28. Since the remaining length of the fiber is unlikely to fit on spool A with an exact number of turns the additional slack was taken up with one loose coil.

With the fiber loaded into the system the butt-coupling was optimized to provide maximum intensity on the spectral analyzer. The temporary connector was removed from the spectral analyzer and the fiber end inspected with a fiber microscope to confirm that light was coupled into the core and not the cladding or supporting glass structure.

With light verified as propagating in the core of the test fiber the termination connector was re-inserted into the spectral analyzer and an appropriate integration time chosen to maximize the detected signal without saturation.

The strain on spool C was removed while the jaw separation was moved to the minimum distance (10 mm) and re-applied.

A LabView program automatically increased the jaw separation in 0.25 mm steps from 10 mm to 159.75 mm for a total of 600 individual transmission spectra. Once complete the

Optics EXPRESS

tungsten lamp was switched off and a background spectra recorded with the same integration time and averaged over 10 spectra.

The measured data were processed automatically using a purpose written Mathematica program. The first step was to ascertain the maximum transmitted power at each wavelength over all bend diameters. With the background subtracted, this was used as the reference transmission and thus loss (in dB) was calculated for according to Eq. (1):

$$A(\varphi,\lambda) = 10\log_{10}\left[\frac{I(\varphi,\lambda)_m - I(\lambda)_b}{I(\lambda)_r - I(\lambda)_b}\right], \tag{1}$$

where $A(\phi,\lambda)$ is the loss of a single 180° bend as a function of bend diameter, ϕ, and wavelength, λ, and I is wavelength dependent intensity recorded for: the measured bend diameter, m, background intensity, b, and reference (maximum measured intensity over all bend diameters), r.

5. Analytical model

In AR-HCF, the effective refractive index of an $LP_{l,m}$ mode propagating in either the core or one of the cladding capillaries can be approximated by Marcatili-Schmelzer's model [8] Eq. (2):

$$n_{l,m}(\lambda) = 1 - \frac{1}{2}\left(\frac{j_{l,m}\lambda}{2\pi r}\right)^2, \tag{2}$$

where r is the effective radius of 'air' region in either the core or a cladding capillary; $j_{l,m}$ is the m'th zero of the Bessel function of the first kind, J_l ; and λ is the wavelength.

Using a conformal transformation, the relative phase lagging in a bent fiber along the bend radius direction is equivalent to a redistribution of refractive index in another straight fiber [22]. Similarly derived as [11, 12], the critical bend radius of specific resonant bend losses corresponding to the coupling of a specific core mode to a specific cladding capillary mode can then be approximately expressed as Eq. (3):

$$R_{j,l,m} = d_j \Big/ \left(\sqrt{\frac{n_{l,m}(\lambda)_{core}}{n_{l,m}(\lambda)_{clading}}} - 1\right), \tag{3}$$

where d_c is the distance between the center of the core and the c^{th} capillary projected onto the plane of the bend Fig. 4, while $n_{l,m}(\lambda)_{core}$ and $n_{l,m}(\lambda)_{cladding}$ are the effective indices of two specific core and cladding capillary modes in a straight fiber calculated from Eq. (2). Note that for C capillaries there are C equivalent distances for any given bend plane. Hence each resonance condition corresponds to a specific LP mode in the core coupling to a specific LP mode in a specific, c^{th}, capillary with a specific angle, θ, to the bend plane (Fig. 4).

Optics EXPRESS

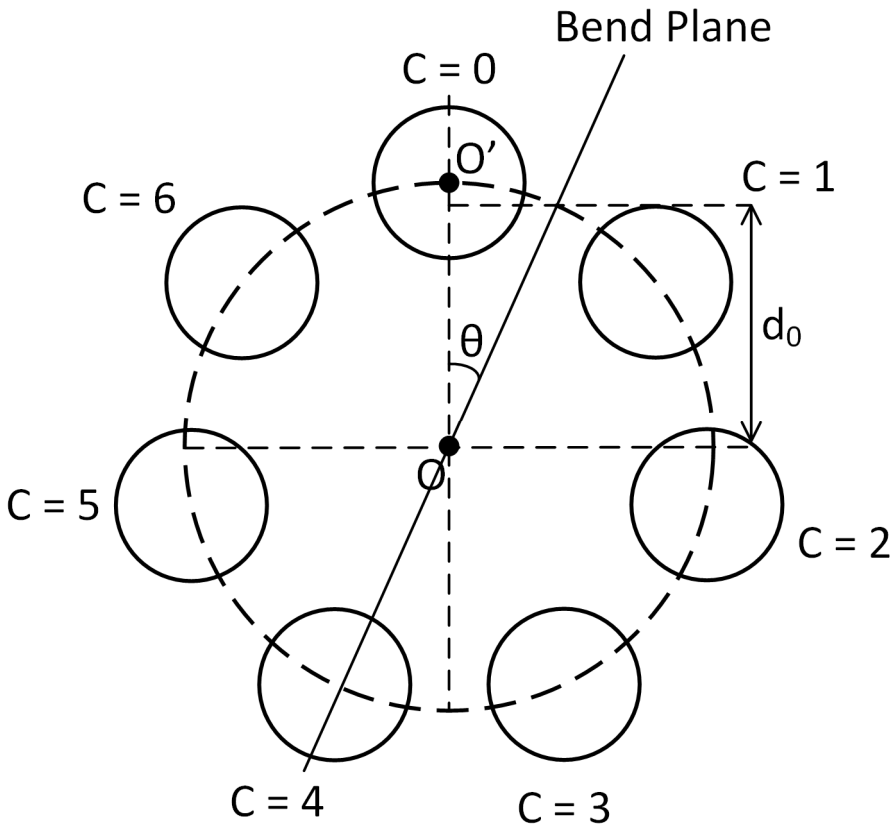

Fig. 4. Illustration of an 7 cell (C = 7) fiber structure as used for the analytical model. O is the center of fiber core and O' is the center of the 0th capillary. With a bend direction along the black line the equivalent distance between the centers of a core and cladding, *d*, may be expressed as $\overline{OO'}\cos(\theta)$.

6. Results and discussion

Plots of the measured bend dependent attenuations are shown in Fig. 5 left. In each case it is possible to see clear specific resonances as well as the edges of the fiber transmission window (which appear as noise in the processed data). The calculated bend loss resonance diameters (using Eq. (3) are shown in Fig. 5 right. For simplicity the analytical model has assumed:

(i) That the bend plane and fiber structure are aligned (i.e. θ = 0 rad).

(ii) That only the fundamental $LP_{0,1}$ mode is present in the fiber core.

(iii) That only the first ten non-degenerate cladding ring modes need to be considered.

Thus the analytical model is only capable of predicting the trend and overall range of bend diameters in which resonant bands are expected to occur (the envelope) rather than exact positions of the resonance bands. Note that for these fibers coupling only occurs to the c = 0, c = 1 and c = 6 capillaries (where these capillaries are on the outside of the bend) and that due to angular alignment from assumption (i) above the c = 1 and c = 6 curves are degenerate by reason of symmetry.

Optics EXPRESS

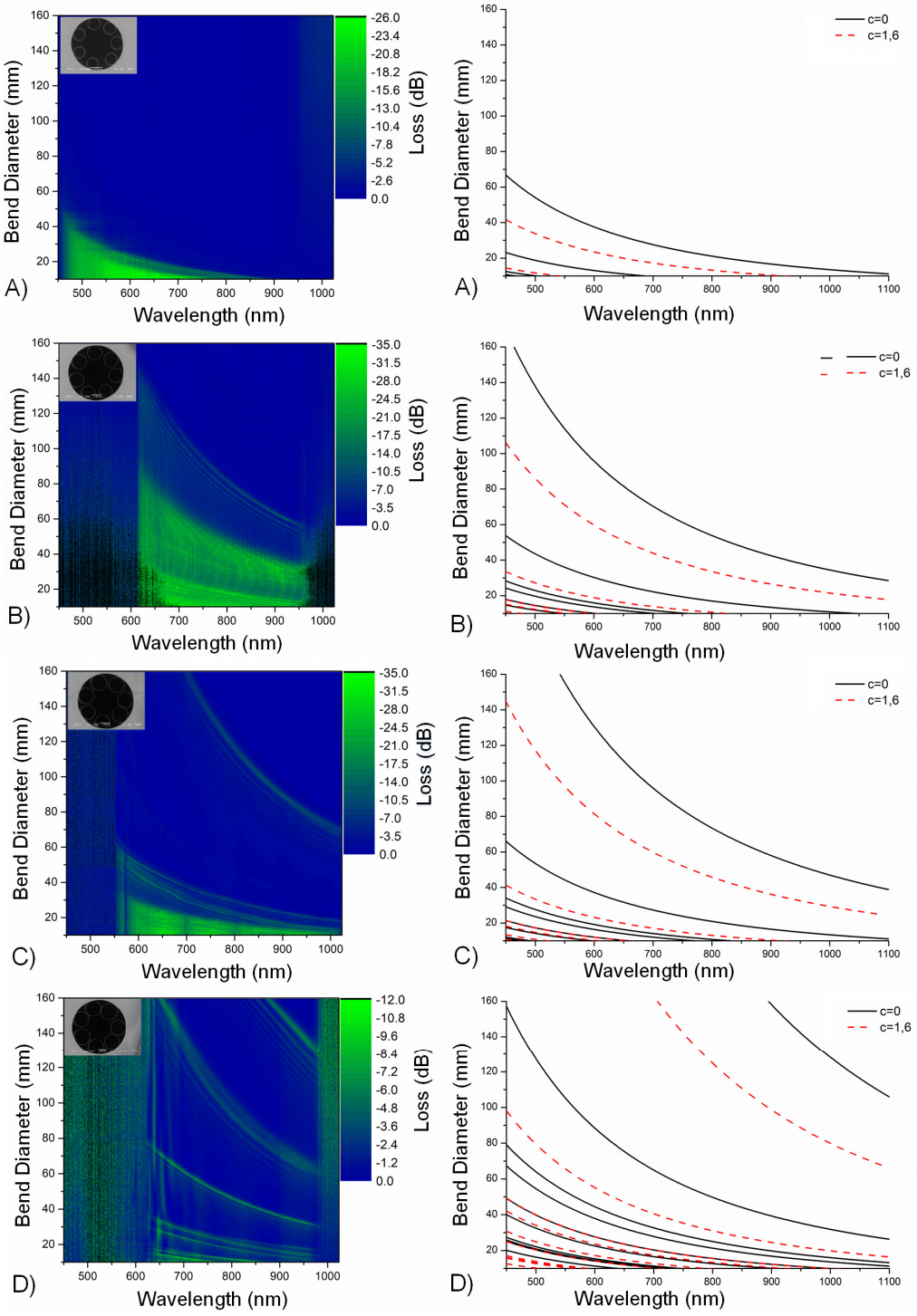

Fig. 5. Experimentally measured (left) and theoretically calculated (right) resonant loss bands in the anti-resonant fibers. An SEM image of each fiber has been included as an inset for reference. As the cladding mode order increases, the resonance band shifts to lower bend diameters.

Optics EXPRESS

Nevertheless, experimental and analytical data show good agreement in the number of resonance bands and particularly in the range of resonant coupling wavelengths, i.e. the overall envelope. However the experimental data shows a more complex structure with several sub bands associated with each predicted resonance at lower bend diameters than the main loss band which are likely the result of more complex inter-modal interference than has been simulated with this simple model.

Of particular note here is that the boundary of the resonance envelope (i.e. minimum lossless bend diameter as a function of wavelength) depends on the ratio between core and cladding sizes; i.e. by decreasing the cladding capillary to core ratio it is possible to significantly suppress resonant losses associated with bending the fiber.

As predicted by the analytical model, repeated measurements on the same fiber with the introduction of an angular alignment offset between bend and fiber orientation (θ) the exact resonance positions are subject to variation, Fig. 6 left. Although the general trends and envelope of resonant bands remains unaffected there is evidence of band splitting, merging and shifting.

This behavior is readily explained by the analytical model, Fig. 6 right. While the resonant position of the $c = 0$ bands do not significantly shift with small variations of θ the $c = 1$ and $c = 6$ bands are no longer degenerate. Instead they split and move in opposite directions resulting in significant mobility in these loss bands depending on the exact angular orientation in the fiber.

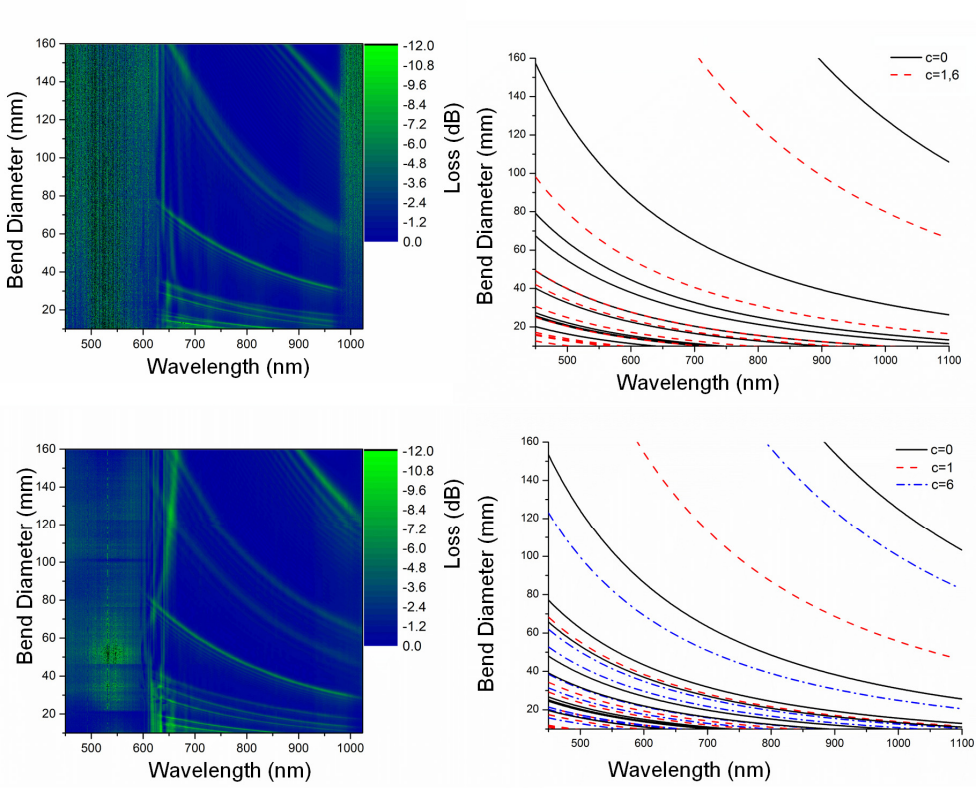

Fig. 6. Left, experimentally measured loss bands in fiber D at two, unknown, angular orientations, θ, cf. Fig. 4. Right: analytical simulation of the effect of angular orientation, top θ = 0 rad, bottom one quarter shift, (θ = ½ π/7 rad). As the angular orientation becomes non-zero the c = 1 and c = 6 resonances split and move apart while the c = 0 resonances are comparatively stable.

Optics EXPRESS

7. Conclusions

In this paper we have presented experimental measurements of the resonant inter-modal bend losses of anti-resonant optical fibers operating in the near infra-red region with results in good agreement with analytical simulations. Theoretical expectations on the effect of the plane of the bend in respect to the fiber geometry (angular orientation) have also been tested and demonstrated to be in broad agreement with experimental observations. The large shifts in precise resonance position, within the overall resonance envelope, demonstrate that it is either necessary to exactly measure the orientation of the fiber in respect to the bend plane or (as is more practical) to ensure that the bend diameter is always greater than the resonance envelope (i.e. above the critical bend radius of the $LP_{0,1}$, $c = 0$, $\theta = 0$ cladding mode [12]) by using an appropriate cabling solution.

It has also been demonstrated that, as the ratio of cladding capillary diameter: core diameter decreases, the critical bend radius and thus the range of resonant bend diameters is suppressed to lower bend diameters. With a ratio of 0.70, resonances are clearly visible up to bend diameters above 160 mm at 800 nm while decreasing the ratio to 0.43 suppresses the lowest order resonance to bend a bend diameter of ~15 mm at 800 nm. This demonstrates that for practical applications care must be taken in fiber design to limit the impact of resonant coupling.

Funding

Engineering and Physical Sciences Research Council (EPSRC) (EP/M025381/1, EP/I01246X/1, EP/M025888/1, EP/I01246K/1)

Acknowledgments

Supporting data are available from the Heriot-Watt Research Portal https://researchportal.hw.ac.uk and used under a Creative Commons Attribution License.